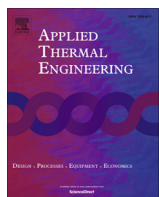




ELSEVIER

Contents lists available at ScienceDirect

Applied Thermal Engineering

journal homepage: www.elsevier.com/locate/apthermeng

Research Paper

Numerical study of monodispersed particle deposition rates in variable-section ducts with different expanding or contracting ratios



Hao Lu, Lin Lu*, Yu Jiang

Department of Building Services Engineering, The Hong Kong Polytechnic University, Hung Hom, Kowloon, Hong Kong, China

HIGHLIGHTS

- The numerical model is validated with experimental results for uniform-section duct.
- Particle deposition rate keeps increasing with the increase of particle size in contracting duct.
- 20–30 μm particles have the maximum deposition velocities in expanding duct.
- “Particle free zone” appears in expanding duct but not exists in contracting duct.
- Particle deposition mechanisms in variable-section ducts are analyzed and discussed.

ARTICLE INFO

Article history:

Received 3 June 2016
Revised 16 August 2016
Accepted 26 August 2016
Available online 28 August 2016

Keywords:
Particle deposition
Variable-section duct
CFD
Numerical simulation

ABSTRACT

This paper presents the deposition rates of monodispersed particle in variable-section ducts with different expanding and contracting ratios. The Eulerian-Lagrangian approach based on Reynolds stress model (RSM) with turbulent fluctuation correction and discrete particle model (DPM) was adopted to investigate particle deposition behaviors in ducts. Particle deposition velocity profile in uniform-section duct was first predicted and validated well with the literature data. Then, particle deposition velocities, air flow field structures, particle trajectories and deposition mechanisms in variable-section ducts with different expanding and contracting ratios were investigated and analyzed in details. For expanding duct cases, particle deposition velocity first keeps constant, then greatly increases, finally decreases with the increase of particle size. The maximum particle deposition rate appears for 20–30 μm particles. As the growth of expanding ratio, the particle deposition velocities are significantly reduced for $d_p > 5 \mu\text{m}$ while almost not affected for $d_p < 5 \mu\text{m}$. For contracting duct cases, particle deposition velocity keeps increasing when particle size increases. Moreover, particle deposition velocities are greatly increased for $d_p < 30 \mu\text{m}$ but very closed for $d_p > 30 \mu\text{m}$, when the contracting ratio increases. The modification of deposition distance, the variation of air velocity along the streamwise direction as well as air flow structures are the main mechanisms to change the particle deposition characteristics, compared with uniform duct case. Besides, the “particle free zone” appears for large particles in expanding duct cases while it doesn't exist for contracting duct cases.

© 2016 Elsevier Ltd. All rights reserved.

1. Introduction

Aerosol particle transport and deposition in building ventilation ducts are crucial for indoor air quality (IAQ) [1–3]. In the building ventilation system, variable cross-section ducts are usually common, such as expanding and contracting ones. Particle deposition rate and mechanism in varying-section ducts may be very different from those in uniform duct, as the geometrical configuration and flow field structures are greatly modified. However, according to

authors' knowledge, very limited researches have been conducted on particle deposition in expanding or contracting ducts. Thus, it is necessary to carefully investigate this issue.

This study was focused on deposition behaviors of monodispersed particle. In the past several decades, a large number of researches have been carried out on monodispersed particle deposition behaviors in uniform ducts, including experimental studies [4–8], theoretical analysis [9–12] and numerical simulations [13–24]. It was found that particle deposition rate profile for vertical duct case can be divided into turbulent particle diffusion regime, eddy diffusion-impaction regime and inertia-moderated regime with the increase of particle relaxation time [4–7]. In the

* Corresponding author.

E-mail address: vivien.lu@polyu.edu.hk (L. Lu).

Nomenclature

C_0	mean particle concentration	u'_{rms}	streamwise fluctuating velocity of air
D_1	uniform duct width	V_d	particle deposition velocity
D_2	outlet width of expanding duct	V_d^+	dimensionless particle deposition velocity
D_3	outlet width of contracting duct	v'_{rms}	wall-normal fluctuating velocity of air
F_S	Saffman's lift force	w'_{rms}	spanwise fluctuating velocity of air
f	fanning friction factor	u^*	frictional velocity of air
h	duct height	y^+	dimensionless distance from the wall
J	number of particles deposited per unit time and unit area		
k	turbulent kinetic energy (T.K.E.)		
\bar{p}	time-averaged pressure		
Re	Reynolds number		
S	ratio of particle-to-fluid density		
U_{mean}	mean velocity of air		
U_{free}	freestream velocity of air		
u_g	velocity of fluid		
\bar{u}_i	time-averaged velocity		
u_p	velocity of particle		
			<i>Greek symbols</i>
		ε	dissipation rate of turbulent kinetic energy
		ρ_g	density of fluid
		ρ_p	density of particle
		ζ	normal distributed random number
		μ	dynamic viscosity of air
		ν	kinetic viscosity of air
		τ_p^+	dimensionless particle relaxation time
		λ_e	expanding ratio of duct inlet and outlet diameter
		λ_c	contracting ratio of duct inlet and outlet diameter

first regime, deposition behaviors of particles are mainly determined by turbulent eddy and Brownian diffusions. In the second one, particle deposition is controlled by the motions of turbulent eddies and particle inertia. In the last one, the particle inertia is the main mechanism of deposition. Considering Brownian diffusion, turbulent diffusion and gravity settling, the “three-layer” model was developed to predict deposition rate of particles on smooth surface by Lai and Nazaroff [10]. Further, this model was revised to successfully predict particle deposition rate in smooth and rough uniform ducts by Zhao and Wu by considering turbophoresis [11,12]. Except for experimental and theoretical studies, a large number of numerical simulations based on the CFD (computational fluid dynamics) have been conducted to investigate particle deposition in uniform duct [13–24]. There are two main numerical methods on this issue, i.e. the Eulerian-Eulerian and the Eulerian-Lagrangian approaches. The former one considers particles as continuous phase and establishes transport equations as fluid phase. Zhao and Chen [13] successfully predict particle deposition velocity in uniform ventilation duct by the Eulerian-Eulerian method. The latter one obtains the spatial particle positions and instantaneous particle velocities by tracking the trajectories of each particle. It was found that the RSM (Reynolds stress model) with correction of turbulent velocity fluctuation can accurately predict particle deposition rate in uniform duct by Tian and Ahmadi [14], Gao et al. [15], because RSM considers turbulent anisotropy. Moreover, Zhang and Chen [16] also accurately simulated particle deposition behaviors in uniform ventilation duct by $\bar{v}^2 - f$ turbulent model with a modified Lagrangian method.

Nevertheless, studies on monodispersed particle deposition in variable-section duct was very limited. Haber et al. [25] and Lee and Lee [26] investigated particle deposition in expanding and contracting alveolus by CFD methods. The results showed that particle deposition is enhanced by turbulent motions in the near-wall regions. Moreover, particle deposition behaviors in S-connector and duct bend were experimentally studied by Sippola and Nazaroff [27–29] in details. It was also found that particle deposition rate is significantly increased compared with uniform duct case. However, particle deposition in variable-section ducts with different expanding and contracting ratios has never been investigated. The deposition characteristics and mechanisms in variable-section ducts remain unclear. Therefore, this study aims to investigate the deposition behaviors and mechanisms of monodispersed particles

in variable-section ducts by CFD simulation. The effects of different expanding and contracting ratios of the duct on particle deposition rate and air flow fields would be studied in details, and the results will be compared with the ones of uniform duct case.

2. Numerical models

2.1. RSM model and DPM model

In present study, RSM (Reynolds stress model) was adopted to predict turbulent air flow fields in variable-section ducts, as its accuracy for particle deposition has been proved by many researches [14,15]. At the same time, DPM (discrete particle model) was employed to simulate particle deposition behaviors in ducts. Correction of wall-normal turbulent velocity fluctuation was conducted for both the uniform- and variable-section duct flows to ensure the accuracy of simulation.

For air flow in ducts, RSM model was adopted in the simulation. The Reynolds-Averaged Navier-Stokes equations and the Reynolds stress transport equation were resolved to predict turbulent air flow fields. Moreover, the turbulent flow fields in the near-wall regions were modeled by the two-layer zonal model with enhanced wall function [20]. More details of RSM model and two-layer zonal model can be found in the authors' previous studies [2,3].

For particle motion, DPM (discrete particle model) was employed to track the trajectory of each particle. Dilute gas-particle flow was considered in this study, thus the effect of particle behaviors on air flow fields and inter-particle interaction were ignored in the simulation. Zhao and Chen [30] found that the Bas-set, the virtual and the pressure gradient forces are small enough to be ignored when air to particle density ratio is quite small. Therefore, the drag, the gravity, the buoyancy, the Brownian and the Saffman's lift forces were considered in this simulation. The governing equation of particles can be written by,

$$\frac{du_p}{dt} = \frac{1}{\tau} \frac{C_D Re_p}{24} (u_g - u_p) + \frac{g(\rho_p - \rho_g)}{\rho_p} + \zeta \sqrt{\frac{\pi S_0}{\Delta t}} + \frac{2\rho K_c v^{0.5}}{\rho_p d_p (S_{lk} S_{kl})} s_{ij} (u - u_p) \quad (1)$$

The drag coefficient C_D is computed as follows,

$$C_D = \begin{cases} \frac{24}{Re_p}, & \text{for } Re_p < 1 \\ \frac{24}{Re_p}(1 + 0.15Re_p^{0.687}), & \text{for } 1 < Re_p < 400 \end{cases} \quad (2)$$

The particle deposition velocity can be estimated as follows [14,16],

$$V_d = \frac{J}{C_0} = \frac{N_d/t/A}{N_0/V} \quad (3)$$

where J is the number of deposited particles per unit time and unit surface area. C_0 is mean particle concentration. The dimensionless particle deposition velocity is computed by,

$$V_d^+ = \frac{V_d}{u^*} \quad (4)$$

where u^* is the friction velocity.

The dimensionless particle relaxation time is a time scale characterizing the adjustment of particle velocity to a changing fluid velocity [14]. It can be calculated by,

$$\tau_p^+ = \frac{C_C S d_p^2 u^{*2}}{18 \nu^2} \quad (5)$$

2.2. DRW model and turbulent fluctuation correction

Turbulent dispersion of particle is an important mechanism for deposition, especially in near-wall region. DRW (discrete random walk) model is commonly adopted to model the turbulent particle dispersion [14–16]. A Gaussian distributed random fluid velocity fluctuation and a time scale of turbulent eddy are adopted in this model [31]. For RSM model, the instantaneous velocity fluctuation of the fluids can be described by,

$$u' = \zeta u'_{rms}, \quad v' = \zeta v'_{rms}, \quad w' = \zeta w'_{rms} \quad (6)$$

where u'_{rms} , v'_{rms} and w'_{rms} are the fluid velocity fluctuation. ζ is normal distributed random number.

However, previous studies indicated that wall-normal turbulent fluctuation in the near-wall region is crucial for accurately predicting the particle deposition velocity [14–16]. Particle deposition velocity would be over-predicted by the RSM model, especially in the diffusion-impaction regime [14–16]. In present simulation, the wall-normal turbulent fluctuation was corrected by direction numerical simulation (DNS) results [32] in the near-wall region for uniform duct case, as shown in Eq. (7)

$$\frac{v'_{rms}}{u^*} = C(y^+)^2, \quad \text{for } y^+ < 4 \quad (7)$$

In Eq. (7), $C = 0.008$. u^* is the friction velocity. y^+ is the non-dimensional distance from the wall. Moreover, the wall-normal turbulent velocity fluctuation was also corrected by Eq. (8) for variable-section duct cases,

$$\frac{v'_{rms}}{u^*} = \frac{a_1 y^{+2}}{1 + b_1 y^+ + c_1 y^{+2.41}}, \quad \text{for } y^+ < 30 \quad (8)$$

In Eq. (8), $a_1 = 0.0116$, $b_1 = 0.203$ and $c_1 = 0.0014$. This equation has been applied to simulate particle deposition in complex geometry such as human mouth and ribbed duct [33,34].

3. Case description and solution strategy

3.1. Computational domain

Fig. 1 shows the schematic of aerosol particle deposition in uniform- and variable-section ducts. The two-dimensional uniform-section duct is 0.4 m long and 0.02 m wide, as shown in Fig. 1(a). This geometry parameter has been widely adopted for

studying the particle deposition in uniform duct [14–16], and there are a large number of experimental and numerical data for validation in literatures. Tian and Ahmadi [14] and Gao et al. [15] numerically investigated monodispersed particle deposition in uniform-section duct by CFD method. In their studies, the first half of the duct was designed to ensure full development of turbulent air flow, and particles were released at the mid-section of duct. In order to agree with the cases of Tian et al. and Gao et al., the first half of ducts were designed to ensure full development of air flow in uniform, expanding and contracting cases. The length of L1, L2 and L3 in Fig. 1 is all 0.2 m. Three expanding ratios λ_e were investigated, i.e. 1:1.5, 1:2 and 1:2.5. Fig. 1(c) is for the contacting duct case. The contracting ratios of the ducts λ_c are 1.5:1; 2:1 and 2.5:1.

3.2. Structural grids

Structured grids were established to discretize the computational domain for both uniform- and variable-section ducts. The first grid spacing from the wall was found to be crucial for simulating particle deposition rate. Tian and Ahmadi [14] investigated the influences of several different grid solutions and first grid spacing from the duct wall on the prediction results. The first grid spacing were 0.1, 0.05, 0.01, 0.005, 0.001 and 0.0005 mm away from the wall. The results showed that the accurate prediction compared with experimental data can be obtained when the first grid spacing is 0.05 mm and the grid growing factor is 1.2 from the walls to the core regions. In this study, the grid independence check was not conducted repeatedly. This grid solution of Tian and Ahmadi [14] was adopted in this paper. For uniform- and variable-section ducts, the computational grid number are both 32,000. In order to display the mesh more clearly, only part of the grids of three kinds of ducts were enlarged and shown in Fig. 2. The computational grids are showed in Fig. 2(a), (b) and (c) for uniform- and variable-section ducts, respectively.

3.3. Boundary conditions

Boundary conditions have great influence on computational results. To predict turbulent air flow in ducts more accurately, fully developed velocity and T.K.E. (turbulent kinetic energy) profiles were imposed in the duct inlet for both uniform- and variable-section cases. The fully developed velocity profiles are described by [14],

$$U = U_{free} \left(\frac{y}{D/2} \right)^{1/7} \quad \text{for } y \leq D/2 \quad (9)$$

$$U = U_{free} \left(\frac{h-y}{D/2} \right)^{1/7} \quad \text{for } y > D/2 \quad (10)$$

$$U_{free} = \frac{8}{7} U_{mean} \quad (11)$$

where D is inlet height of the duct. U_{mean} is mean velocity of air flow. Moreover, the fully developed T.K.E. profiles can be demonstrated as follows [14],

$$k = \frac{\tau_w}{\rho_g \sqrt{C_\mu}} + \frac{y}{D/2} \left(0.002 U_{free}^2 - \frac{\tau_w}{\rho_g \sqrt{C_\mu}} \right) \quad \text{for } 0 \leq y \leq D/2 \quad (12)$$

$$k = \frac{\tau_w}{\rho_g \sqrt{C_\mu}} + \frac{D-y}{D/2} \left(0.002 U_{free}^2 - \frac{\tau_w}{\rho_g \sqrt{C_\mu}} \right) \quad \text{for } D/2 < y \leq D \quad (13)$$

$$\tau_w = \frac{\rho_g U_{mean}^2}{2} \cdot f \quad (14)$$

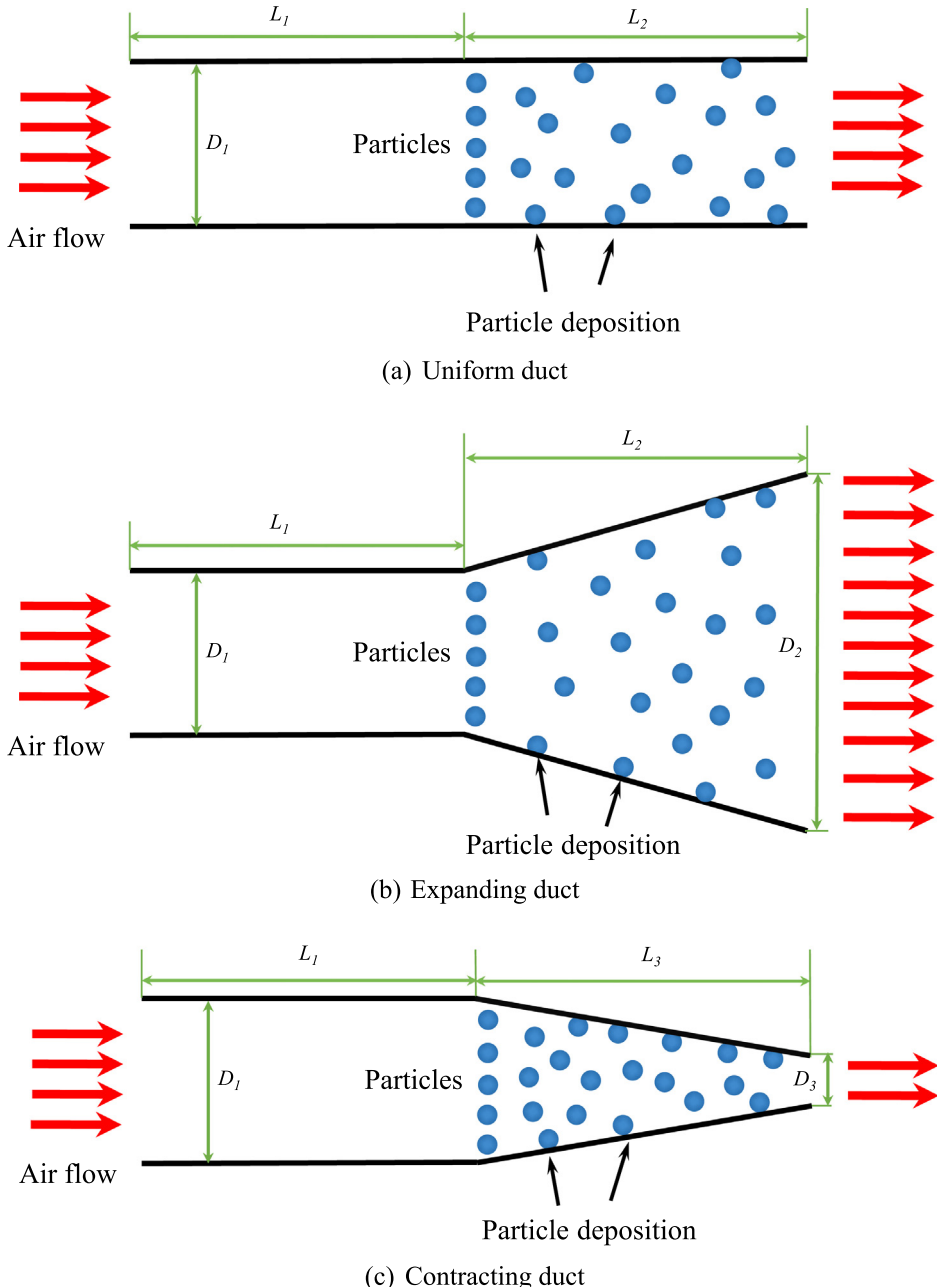


Fig. 1. Schematic view of particle deposition in uniform- and variable-section ducts.

For air flow, non-slip boundary condition was employed on the duct walls. Pressure outlet boundary condition was used at the outlet of the duct. For particle motion, particles were assumed to be deposited on the wall once they contact with the wall. This boundary condition was also used in the literatures for particle deposition in uniform duct [14–16]. Particle rebound from the wall for re-suspension were not considered in the simulation. At the outlet, the particles were set as transported out of the computational domain [35,36].

3.4. Solution strategy

Finite volume method (FVM) and Runge-Kutta method were employed to resolve the air governing equations and particle motion equations. The convection and diffusion terms were discretized by the second-order upwind and the second-order central

difference schemes, respectively. The Semi-Implicit Method for Pressure-Linked Equations (SIMPLE) algorithm [37] was adopted to decouple the pressure and velocity fields. For turbulent air flow, if the residual values of the velocity, Reynolds stress and continuity were less than 1×10^{-6} , the computation was considered to converge. After convergence of air flow, particle motions in the ducts were simulated by DPM model. The deposited particle number would be increased with the increase of the time of particle motion. In a specific time interval, the deposited number of particle was counted and the particle deposition velocity can be calculated. In the simulation, the dynamic viscosity of the air μ is 1.789×10^{-5} kg s/m. The density of the air is 1.225 kg/m³. A total number of 30,000 monodispersed particles were released from the duct middle position after the air flow reaches fully development. The air velocity and initial particle velocity was 5.5 m/s. The Reynolds number of the air flow based on the mean velocity

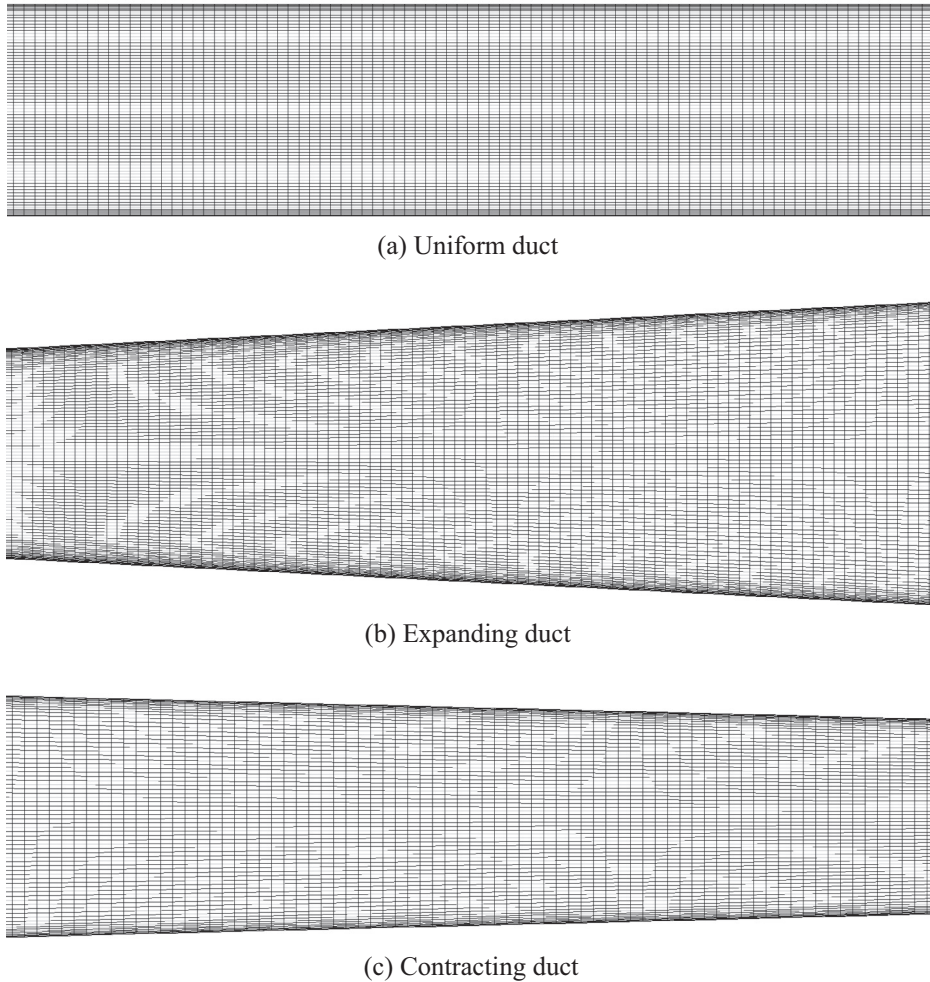


Fig. 2. Partial structural grids for uniform- and variable-section ducts.

and duct height was 7534. The density ratio of particle to fluid S is 2000. Particle sizes are 1, 2, 3, 5, 10, 20, 30 and 50 μm . A total number of 56 cases were investigated in the study, as shown in **Table 1**.

4. Results and discussions

4.1. Air flow fields and numerical validation

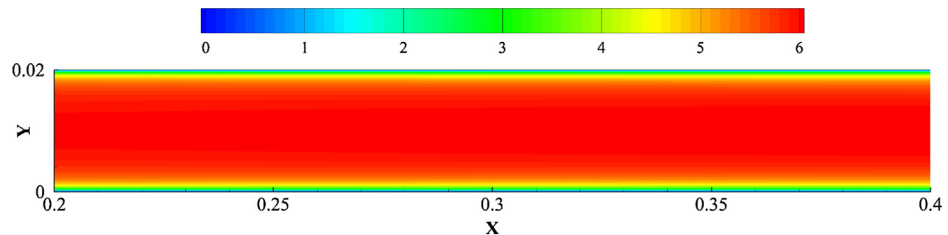
Fig. 3 shows the air velocity fields for the second half of the uniform- and variable-section ducts with different diameter ratios. For uniform duct case, there is only velocity variation in the near-wall boundary layers, while the air flow velocity remains steady in the main flow regions, as shown in **Fig. 3(a)**. Nevertheless, the air flow fields are more complex in expanding and contracting duct cases. For expanding duct cases, significant air velocity differences

can be seen in the whole flow fields. The air velocity is decelerated along the streamwise direction, as shown in **Fig. 3(b)**. On the contrary, the air velocity is obviously accelerated in flow direction for contracting duct cases. These tendencies are enhanced when the expanding or contracting ratios of the ducts are increased. The complicated air flow fields may result in more complex particle deposition behaviors.

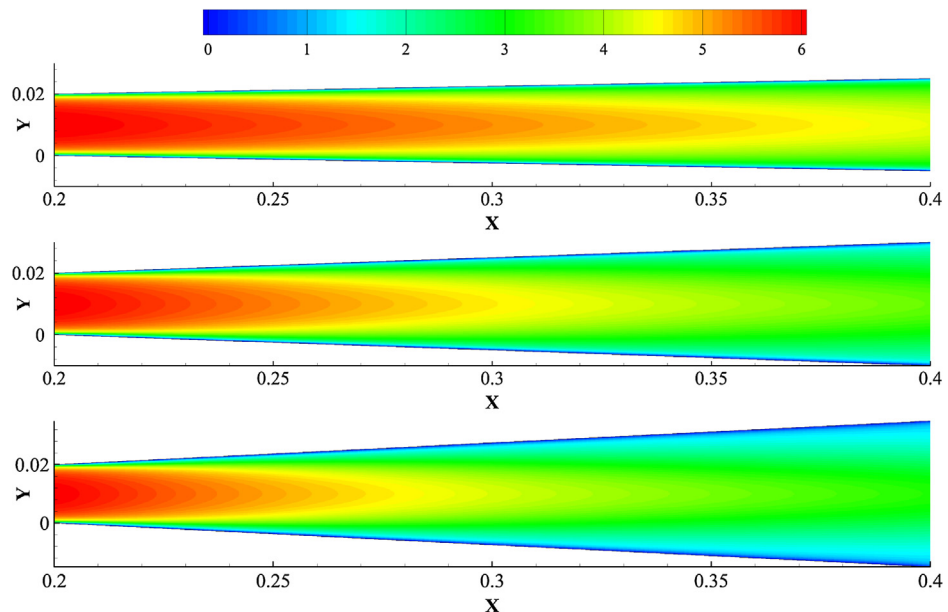
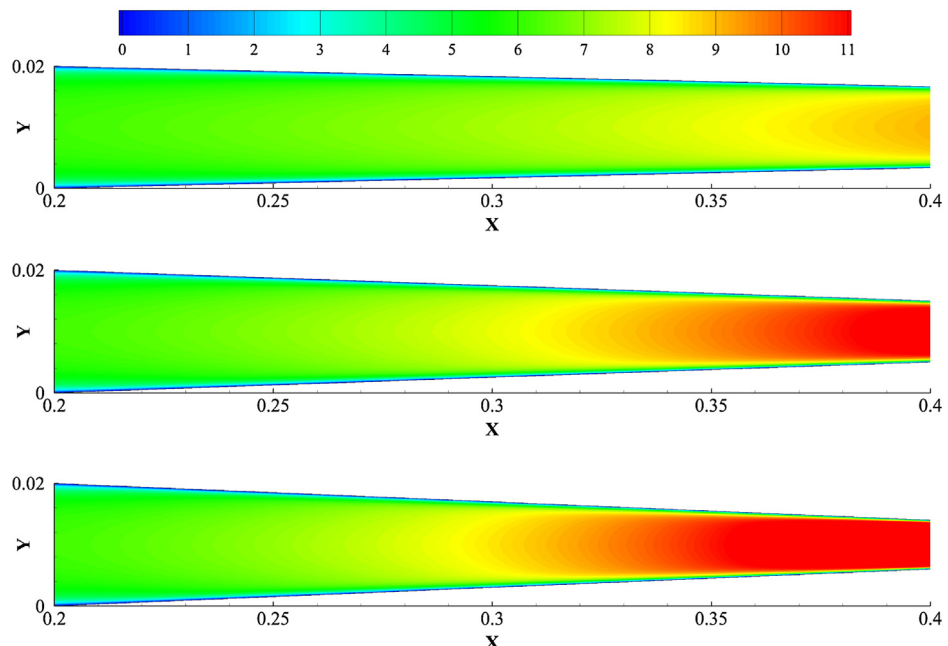
To validate the numerical method, **Fig. 4** shows validation of air flow velocity and particle deposition velocity for uniform duct case. The mean and fluctuating velocity profiles of air flow in uniform duct were validated with DNS data by Kim et al. [32], as shown in **Fig. 4(a)** and (b), respectively. From **Fig. 4(a)**, it can be observed that the mean air velocity is in good agreement with the DNS results. From **Fig. 4(b)**, the streamwise velocity agrees roughly with the DNS results. However, the fluctuating velocity profile in

Table 1
Computational cases.

Case no.	Air velocity (m/s)	Particle diameter (μm)	Duct type	Diameter ratio
S (1–8)	5.5	1, 2, 3, 5, 10, 20, 30, 50	Uniform	–
E1 (9–16)	5.5	1, 2, 3, 5, 10, 20, 30, 50	Expanding	1:1.5
E2 (17–24)	5.5	1, 2, 3, 5, 10, 20, 30, 50	Expanding	1:2.0
E3 (25–32)	5.5	1, 2, 3, 5, 10, 20, 30, 50	Expanding	1:2.5
C1 (33–40)	5.5	1, 2, 3, 5, 10, 20, 30, 50	Contracting	1.5:1
C1 (41–48)	5.5	1, 2, 3, 5, 10, 20, 30, 50	Contracting	2.0:1
C1 (48–56)	5.5	1, 2, 3, 5, 10, 20, 30, 50	Contracting	2.5:1



(a) Uniform duct

(b) Expanding ducts, (From up to down: $\lambda=1.5, 2.0, 2.5$)(c) Contracting ducts, (From up to down: $\lambda=1.5, 2.0, 2.5$)**Fig. 3.** Air velocity fields of uniform- and variable-section ducts with different diameter ratios.

wall-normal direction agrees much better with the literature results after near-wall correction. It was found that the wall-normal turbulent fluctuating velocity is crucial for predicting particle deposition behaviors [14], thus the present turbulent air flow fields are accurate enough for simulating particle deposition. The comparison of present particle deposition velocity profile for uniform duct case with previous experimental and numerical data from the literatures [4–7,14,16,38–40], as shown in Fig. 4(c). The RSM model with and without normal-wall velocity fluctuation correction were both employed to compare the predicting results. It can be seen that the significant difference appears for small particles ($\tau_p^+ < 1$) between the two models, from Fig. 4(c). The deposition rate of small particles would be obviously over-predicted by RSM model without turbulent fluctuation correction. This is because the turbulent particle dispersion is crucial for the deposition of small particles and it's not accurately simulated by RSM model without correction. Nevertheless, the predicting results by RSM model with turbulent velocity fluctuation correction are in very good agreement with the literature data. The agreement indicates that the present numerical models can predict particle deposition in duct very well.

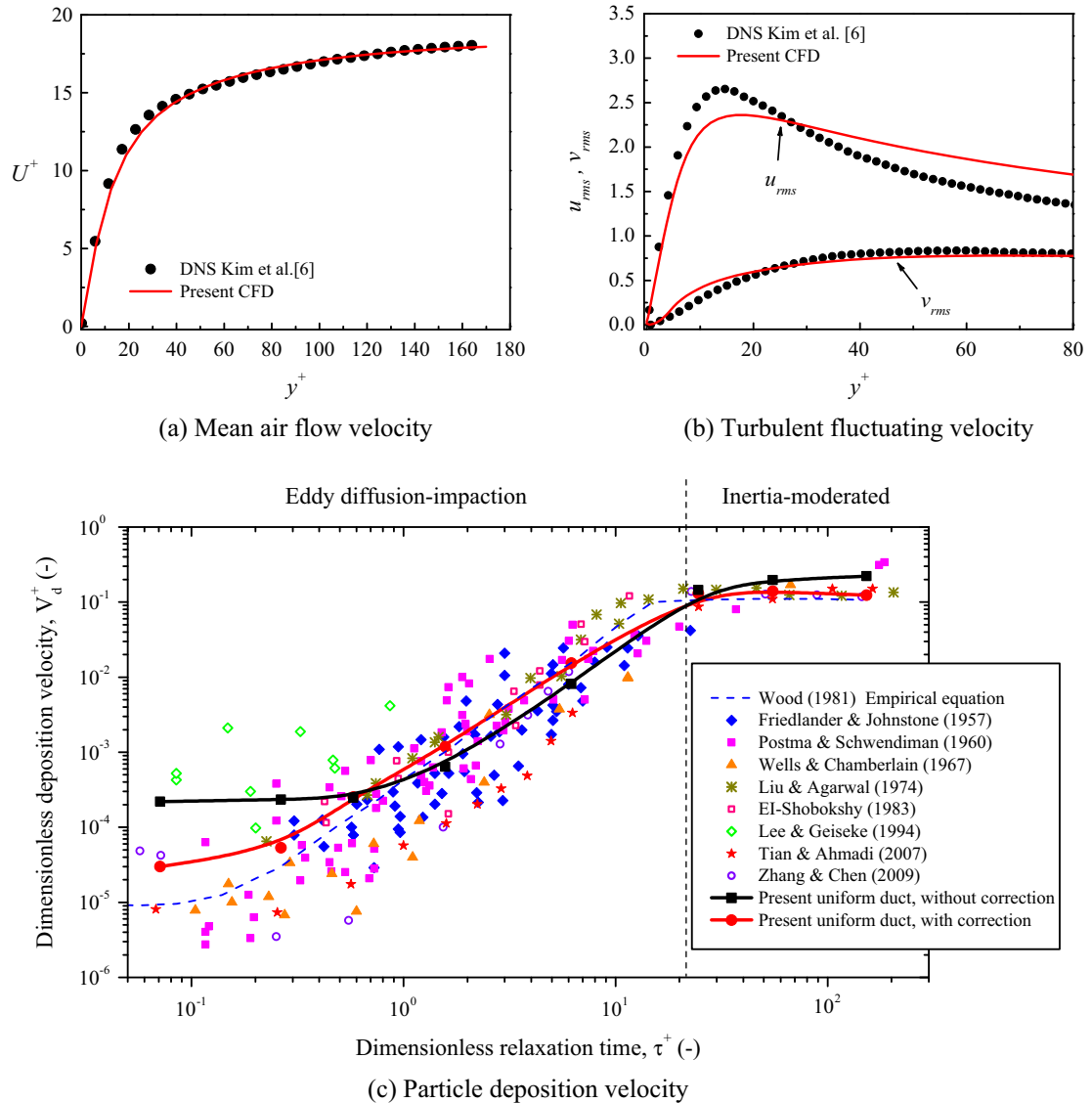


Fig. 4. Validation of air flow velocity and particle deposition velocity for uniform duct case.

4.2. Particle deposition velocity in variable-section ducts

Fig. 5 displays the particle deposition velocity in expanding ducts with different duct diameter ratios. The results were compared with uniform duct case. It can be observed that the particle deposition velocity profiles for expanding duct cases are much different from the uniform duct cases. Although particle deposition velocities for expanding duct cases are overall decreased compared with uniform duct case, the decreasing degrees for different size particles are quite different. This is because the deposition mechanisms are modified when the duct geometry is changed. It can also be concluded from the different shapes of the deposition velocity profiles between the expanding and uniform duct cases. For expanding duct cases, the deposition velocity profile can be divided into three regimes. For $d_p < 5 \mu\text{m}$, the deposition behaviors of particles are mainly controlled by turbulent and Brownian diffusion. The deposition velocity is almost not changed with different particle sizes. For $5 \mu\text{m} < d_p < 30 \mu\text{m}$, the deposition velocity is greatly enhanced for about three to four order of magnitude. This is because the particle deposition is enhanced by combination of turbulent diffusion, inertia-impaction and shear induced lift force.

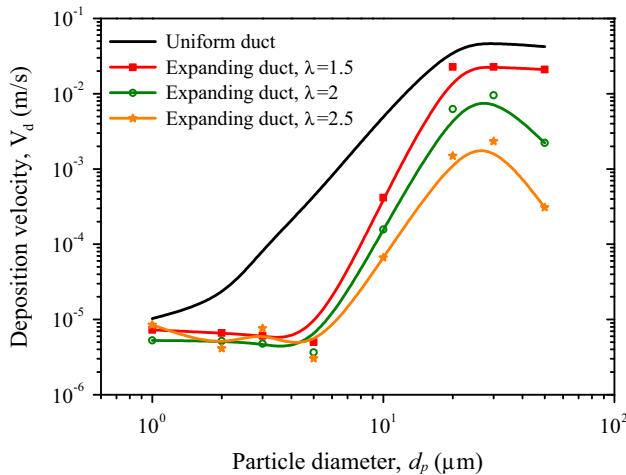


Fig. 5. Particle deposition velocity in expanding ducts with different diameter ratios.

However, the deposition velocity is decreased for $d_p > 30 \mu\text{m}$. This may be caused by the “particle free zone” effect in expanding duct case, as shown in Fig. 8(d). As there are some near-wall regions that the large particles cannot arrive, the deposition velocity is significantly decreased. From the figure, it can be seen that the 20–30 μm particles have the maximum deposition velocities in expanding duct.

For expanding duct cases, it can be seen that the expanding ratio have great influence on particle deposition behaviors, as shown in Fig. 5. Generally, the deposition velocity profile is decreased with the increase of expanding ratio. This is because the deposition distance would be enlarged for larger expanding ratio case. However, the decrease degree of particle deposition velocity is quite different for different particle sizes when the expanding ratio is increased. For $d_p < 5 \mu\text{m}$, particle deposition velocity is almost not affected by the different expanding ratios. This is because turbulent and Brownian diffusion are the main deposition mechanisms for small particles. The particles with small size can be easy to follow the turbulent air flow due to their low inertia. However, the differences of deposition velocity for large particles ($d_p > 5 \mu\text{m}$) are much significant for different expanding ratios. These differences are more obvious with the increase of particle size, as shown in Fig. 5. As particle inertia would be greatly enhanced when particle size is increasing, it's more difficult for large particles to deposit on the duct walls due to the increase of deposition distance.

Fig. 6 shows the particle deposition velocity profiles in contracting ducts with different duct diameter ratios. It can be found that particle deposition velocities in contracting ducts are generally increased compared with the uniform duct case. Different from the uniform duct, particle deposition velocities in contracting ducts are always increased with the increase of particle size. When $d_p < 5 \mu\text{m}$ or $d_p > 30 \mu\text{m}$, the differences of particle deposition velocities are significant between the contracting and uniform duct cases. Nevertheless, for medium particles (about $5 \mu\text{m} < d_p < 30 \mu\text{m}$), relatively small difference can be observed between the two kinds of ducts.

Moreover, when the contracting ratio is increased, the deposition velocity profiles are generally increased due to the reduction of deposition distance. However, the increase degrees of deposition velocity are very different for different particle sizes. For $d_p < 10 \mu\text{m}$, the deposition velocity is significantly increased with the increase of contracting ratios. This is because the TKE value near the wall is enhanced for larger contracting ratio case. The high TKE would enhance the turbulent and Brownian diffusion of the

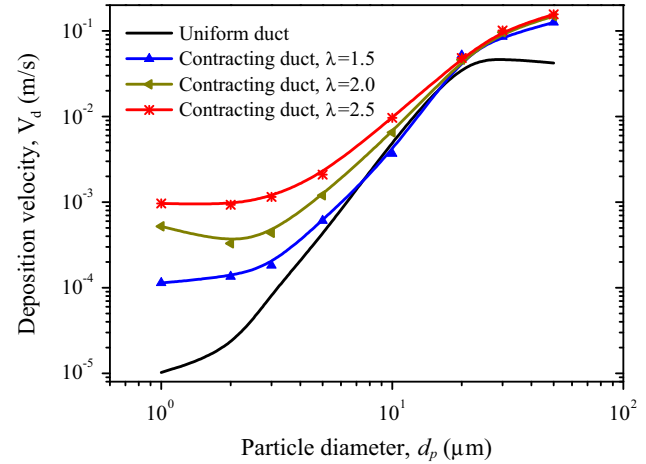


Fig. 6. Particle deposition velocity in contracting ducts with different diameter ratios.

particles. Therefore, the deposition ratio is increased for small particles. Nevertheless, for $d_p > 10 \mu\text{m}$, inertia-impaction is the main mechanism of deposition. The deposition velocity is not obviously modified by the different contracting ratios in the cases of this study. These are quite different from the expanding duct cases. It can be concluded that these deposition characteristics are highly related to the duct geometry, the turbulent flow structures as well as the particle inertia. The detailed particle deposition mechanisms will be discussed by analyzing the T.K.E. distributions and particle trajectories in next section below.

Besides, the effect of different air flow rates on particle deposition is crucial. The influence of different air velocities on deposition velocity of particles in expanding and contracting ducts is shown in Fig. 7. The air velocities in Fig. 7 are 5.5 and 8 m/s. The expanding and contracting ratios are both 2.0. From Fig. 7, it can be observed that particle deposition velocity at 8 m/s is slightly higher than that of 5.5 m/s both for expanding and contracting duct cases. However, the difference becomes very small for large particle sizes (20–50 μm). The main mechanisms of particle deposition are the Brownian diffusion, the turbulent diffusion and the inertia-impaction. The turbulent diffusion would be greatly enhanced with the growth of air velocity, thus the particle deposition velocities are increased accordingly for small particles. However, for large particles, the main mechanism of deposition is inertia-impaction

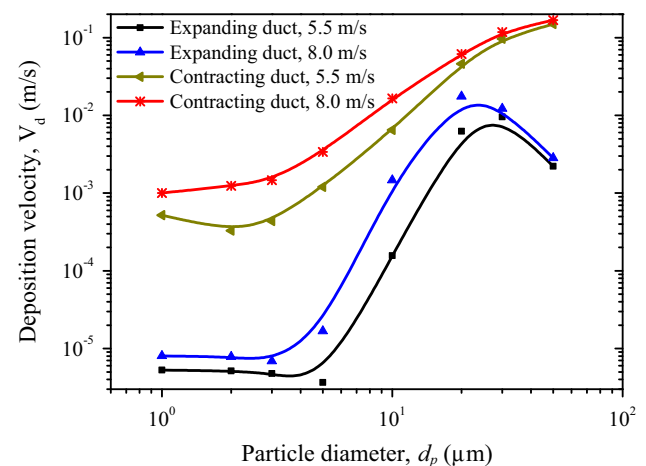


Fig. 7. Effects of different air velocities on particle deposition velocity in variable-section ducts.

but not turbulent diffusion. Therefore, the difference of deposition velocity is not obviously, as shown in the figure. Moreover, the curve shapes of deposition velocity profiles are not modified by different air velocities both for expanding and contracting duct cases. This implies that the deposition mechanisms are the same for different air velocities, although the deposition rates are enhanced for higher air velocity.

4.3. Air flow structures and particle trajectories

To investigate particle deposition mechanisms in variable-section ducts, the T.K.E. distributions and particle trajectories for uniform, expanding and contracting duct cases were demonstrated in Figs. 8–10. The expanding ratio λ_e and contracting ratio λ_c are both 2.5 in Figs. 9 and 10. To observe particle trajectories more clearly, a total number of 30 trajectory samples were randomly selected and displayed in Figs. 8–10. From Fig. 8, it can be observed that the T.K.E. values are quite high in the near-wall regions. Moreover, the streamlines of the air fields are parallel to the flow direction, as shown in Fig. 8(a). Fig. 8(b), (c) and (d) illustrates particle trajectories in uniform duct for 1, 20 and 50 μm particles, respectively. For small particles, it can be found that a large number of particle trajectories are crossed from each other, as shown in Fig. 8(b). This indicates that small particles are easy to modify the motion directions by the turbulent dispersion. However, From Fig. 8(d), these crossed particle trajectories are obviously reduced due to the large inertia of particles. Therefore, the deposition mechanisms between small and large particles are much different.

For expanding duct cases, it can be seen that the near-wall high T.K.E. regions are significantly enlarged compared with uniform duct case, as shown in Fig. 9(a). This may be favorable for deposition of small particles. Nevertheless, the streamlines of air flow are expanding. Thus the deposition distances of particles are increased,

and the distances would be enlarged when the duct expanding ratio is increased. Moreover, the air velocity is decelerated in the flow direction. It means the friction velocity becomes lower along the streamwise direction. It is well known that the friction velocity has important influence on particle deposition velocity. The deceleration of friction velocity would result in the reduction of particle deposition. Therefore, the particle deposition rates for expanding duct cases are overall reduced compared with uniform duct case. Compared the trajectories among 1, 20 and 50 μm particles, significant differences can be observed. The particle trajectories for 1 and 20 μm can be full of the whole flow fields in expanding duct. Nevertheless, the so called “particle free zone” [41–43] was observed for 50 μm particles in the expanding duct. It means that there are some near-wall regions that the large particles cannot arrive. This would cause the decrease of particle deposition velocity for $d_p = 50 \mu\text{m}$. The “particle free zone” phenomenon was previously observed on particle deposition in duct bend [41–43]. As smaller particles could follow the air flow fields very well, thus it's hard to form the “particle free zone”. With the increase of particle size, the “particle free zone” may be induced by the large particle inertia and specific flow structures.

For contracting duct cases, the T.K.E. regions are not obviously enlarged while the T.K.E. values are larger than those for uniform duct case. This means that the small particles are easier to be captured by the near-wall turbulent structures to deposit on the walls. More importantly, the air flow streamlines are contracting along the streamwise direction. It indicates that the deposition distances of particles are reduced. The air flow velocity is increased in the flow direction. The increased friction velocity can also enhance particle deposition rates in ducts. These are all beneficial for particle deposition. From Fig. 10(b)–(d), it can be seen that a lot of particles are intercepted by the contracting duct walls for deposition. Therefore, the contracting duct would enhance particle deposition no matter

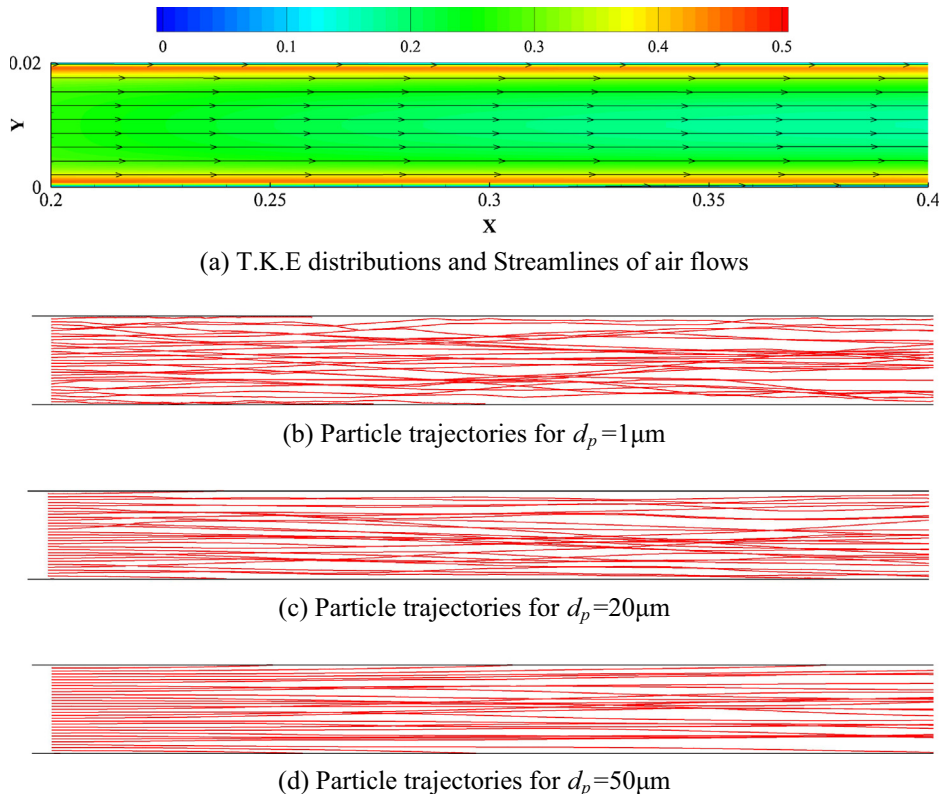


Fig. 8. T.K.E. distributions and particle trajectories in uniform duct.

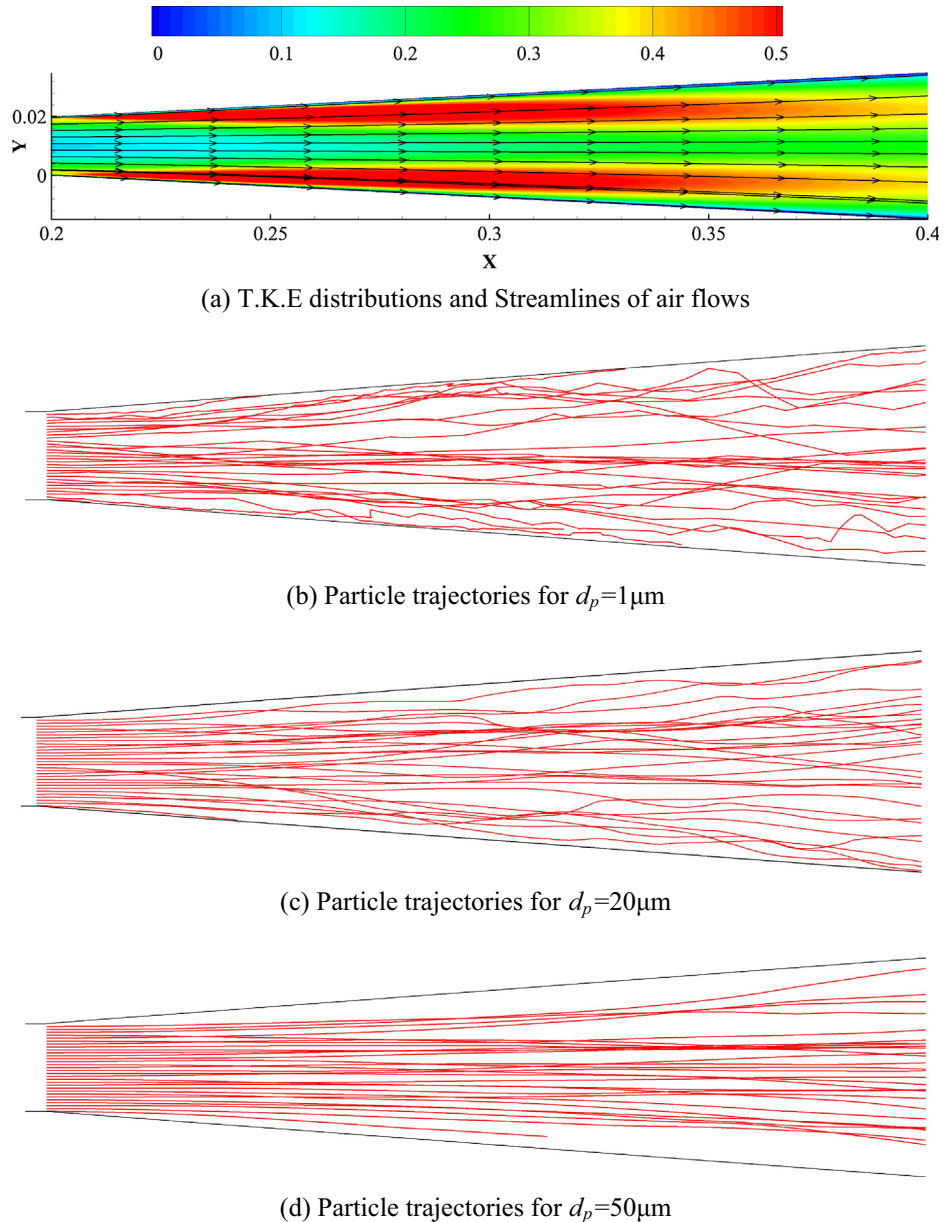


Fig. 9. T.K.E. distributions and particle trajectories in expanding duct with $\lambda_e = 2.5$.

small or large particles. Moreover, it can be observed that no “particle free zone” appears for large particles for contracting duct cases.

5. Conclusions and outlook

Monodispersed particle deposition in variable-section ducts with different expanding and contracting ratios were studied by CFD simulation. After numerical validation, the particle deposition velocities, air flow structures, particle trajectories and particle deposition mechanisms were discussed and analyzed in details. The conclusions can be drawn as follows,

- For expanding duct cases, particle deposition velocity first keeps constant, then greatly increases, finally decreases with the increase of particle size. The maximum particle deposition rate appears for 20–30 μm particles. The decrease of particle deposition velocity for $d_p > 30 \mu\text{m}$ is caused by the “particle free

zone” effect. For $d_p < 5 \mu\text{m}$, particle deposition velocity is almost not affected by the different expanding ratios. However, the deposition velocity is significantly decreased with the increase of expanding ratio for large particles ($d_p > 5 \mu\text{m}$) due to the increase of deposition distance.

- For contracting duct cases, particle deposition velocity always keeps increasing when particle size increases. Moreover, particle deposition velocities are greatly increased with the growth of contracting ratio of duct diameter for $d_p < 30 \mu\text{m}$. While particle deposition velocities are very closed for different contracting ratios for $d_p > 30 \mu\text{m}$.
- The increase of deposition distance and the deceleration of air velocity are the main mechanisms of deposition reduction for expanding duct cases, compared with the uniform duct case. The “particle free zone” appears for 50 μm particles due to large particle inertia and specific flow field structures, while it doesn’t occur for small particles.

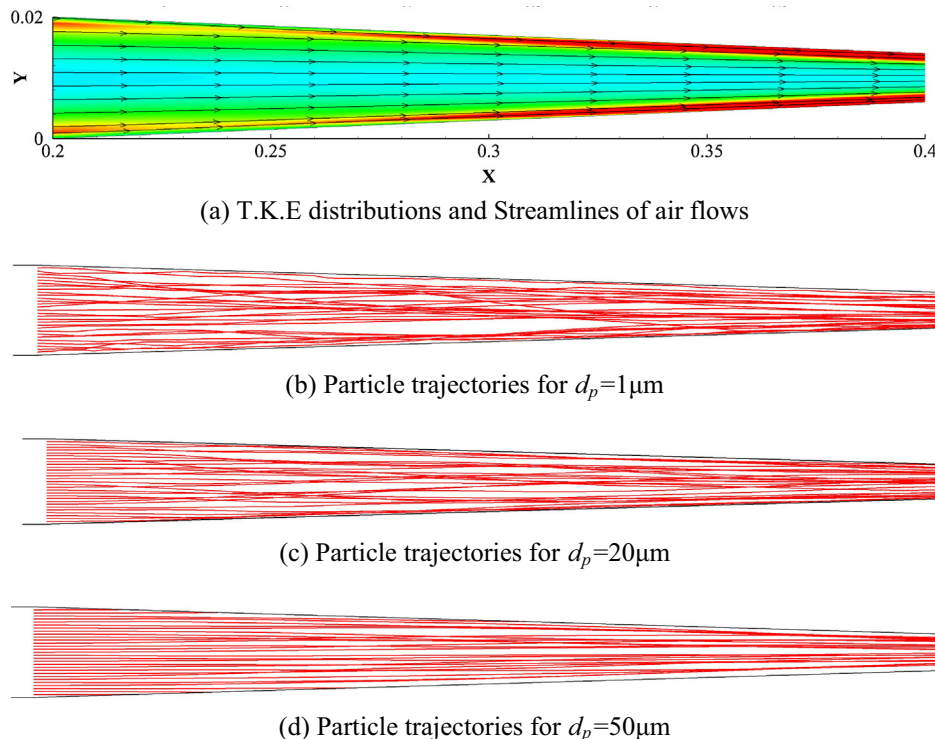


Fig. 10. T.K.E. distributions and particle trajectories in contracting duct with $\lambda_c = 2.5$.

4. On the contrary, the reduction of deposition distance, the acceleration of air velocity and the interception of contracting duct walls would all enhance the particle deposition rates in contracting ducts. No “particle free zone” appears for large particles for contracting duct cases.

The experimental study of particle deposition in variable-section ducts are strongly recommended in future studies. Moreover, it's worth noting that the secondary flow is a crucial phenomenon in the square turbulent duct flow. The effect of secondary flow on particle deposition rates and behaviors needs to be well investigated via experimental study or accurate CFD method such as DNS or LES. Besides, inter-particle collision can be significant for dense gas-particle flow or the regions that particles are greatly clustered. This important issue also needs to be investigated carefully in future work.

Acknowledgements

The authors appreciate the financial supports provided by The Hong Kong Polytechnic University Postdoctoral Fellowships Scheme (G-YWOK) and Central Policy Unit of the Hong Kong Government via the Public Policy Research Scheme (2013.A6.010.13A).

References

- [1] Q. Chen, Ventilation performance prediction for buildings: a method overview and recent applications, *Build. Environ.* 44 (4) (2009) 848–858.
- [2] H. Lu, L. Lu, Numerical investigation on particle deposition enhancement in duct air flow by ribbed wall, *Build. Environ.* 85 (2015) 61–72.
- [3] H. Lu, L. Lu, CFD investigation on particle deposition in aligned and staggered ribbed duct air flows, *Appl. Therm. Eng.* 93 (2016) 697–706.
- [4] A.C. Wells, A.C. Chamberlain, Transport of small particles to vertical surfaces, *Br. J. Appl. Phys.* 18 (1967) 1793–1799.
- [5] B.Y.H. Liu, J.K. Agarwal, Experimental observation of aerosol deposition in turbulent flow, *J. Aerosol Sci.* 5 (1974) 145–155.
- [6] M.S. El-Shabokshy, Experimental measurements of aerosol deposition to smooth and rough surfaces, *Atmos. Environ.* 17 (1983) 639–644.
- [7] K.W. Lee, J.A. Gieseke, Deposition of particles in turbulent pipe flows, *J. Aerosol Sci.* 25 (1994) 699–709.
- [8] G. Da, E. Gehin, M. Ben-Othmane, M. Havet, C. Solliec, C. Motzkus, An experimental approach to measure particle deposition in large circular ventilation ducts, *Environ. Sci. Pollut. Res.* 22 (2015) 4873–4880.
- [9] F. Fan, G. Ahmadi, A sublayer model for turbulent deposition of particles in vertical ducts with smooth and rough surfaces, *J. Aerosol Sci.* 24 (1993) 45–64.
- [10] A.C.K. Lai, W.W. Nazaroff, Modelling indoor particle deposition from turbulent flow onto smooth surfaces, *J. Aerosol Sci.* 31 (2000) 463–476.
- [11] B. Zhao, J. Wu, Modeling particle deposition from fully developed turbulent flow in ventilation duct, *Atmos. Environ.* 40 (2006) 457–466.
- [12] B. Zhao, J. Wu, Modeling particle deposition onto rough walls in ventilation duct, *Atmos. Environ.* 40 (2006) 6918–6927.
- [13] B. Zhao, J.J. Chen, Numerical analysis of particle deposition in ventilation duct, *Build. Environ.* 41 (2006) 710–718.
- [14] L. Tian, G. Ahmadi, Particle deposition in turbulent duct flows – comparisons of different model predictions, *J. Aerosol Sci.* 38 (2007) 377–397.
- [15] N.P. Gao, J.L. Niu, Q.B. He, T. Zhu, J.Z. Wu, Using RANS turbulence models and Lagrangian approach to predict particle deposition in turbulent channel flows, *Build. Environ.* 48 (2012) 206–214.
- [16] Z. Zhang, Q. Chen, Prediction of particle deposition onto indoor surfaces by CFD with a modified Lagrangian method, *Atmos. Environ.* 43 (2009) 319–328.
- [17] N.P. Gao, J.L. Niu, Modeling particle dispersion and deposition in indoor environments, *Atmos. Environ.* 41 (2007) 3862–3876.
- [18] H. Jiang, L. Lu, K. Sun, Simulation of particle deposition in ventilation duct with a particle-wall impact model, *Build. Environ.* 45 (5) (2010) 1184–1191.
- [19] H. Jiang, L. Lu, K. Sun, Computational fluid dynamics (CFD) modelling of particle deposition in a two-dimensional turbulent channel air flow: study of influence factors, *Indoor Built. Environ.* 21 (2) (2012) 264–272.
- [20] K. Sun, L. Lu, H. Jiang, Modelling of particle deposition and rebound behaviour on ventilation ducting wall using an improved wall model, *Indoor Built. Environ.* 20 (3) (2011) 300–312.
- [21] M.B. Othmane, M. Havet, E. Gehin, C. Solliec, Mechanisms of particle deposition in ventilation ducts for a food factory, *Aerosol Sci. Technol.* 44 (2010) 775–784.
- [22] F. Chorvel, A. Kondjoyan, P.S. Mirade, Toward quantitative CFD prediction of contaminant particle deposition against surfaces in large forced-ventilation food plants, *Aerosol Sci. Technol.* 44 (2010) 10–28.
- [23] W.S.J. Uijttewaal, R.V.A. Oliemans, Particle dispersion and deposition in direct numerical and large eddy simulations of vertical flows, *Phys. Fluids* 8 (1996) 2590–2604.
- [24] Y. Wang, P.W. James, On the effect of anisotropy on the turbulent dispersion and deposition of small particles, *Int. J. Multiphase Flow* 25 (1999) 551–558.
- [25] S. Haber, D. Yitzhak, A. Tsuda, Characteristics of particle transport in an expanding or contracting alveolated tube, *J. Appl. Physiol.* 95 (2003) 657–671.
- [26] D.Y. Lee, J.W. Lee, Characteristics of particle transport in an expanding or contracting alveolated tube, *J. Aerosol Sci.* 34 (2003) 1193–1215.

- [27] M.R. Sippola, W.W. Nazaroff, Modeling particle loss in ventilation ducts, *Atmos. Environ.* 37 (2003) 5597–5609.
- [28] M.R. Sippola, W.W. Nazaroff, Experiment measuring particle deposition from fully developed turbulent flow in ventilation ducts, *Aerosol Sci. Technol.* 38 (2004) 914–925.
- [29] M.R. Sippola, W.W. Nazaroff, Particle deposition in ventilation ducts: connectors, bends and developing turbulent flow, *Aerosol Sci. Technol.* 39 (2005) 139–150.
- [30] B. Zhao, Y. Zhang, X.T. Li, X.D. Yang, D.T. Huang, Comparison of indoor aerosol particle concentration and deposition in different ventilated rooms by numerical method, *Build. Environ.* 39 (2004) 1–8.
- [31] FLUENT Inc., FLUENT 12.0 User's Guide, Lebanon, NH, 2009.
- [32] J. Kim, P. Moin, R. Moser, Turbulence statistics in fully developed channel flow at low Reynolds number, *J. Fluid Mech.* 177 (1987) 133–166.
- [33] G. Lericain, S. Drapeau-Martin, T. Barth, U. Hampel, Numerical simulation of multilayer deposition in an obstructed channel flow, *Adv. Powder Technol.* 25 (2014) 310–320.
- [34] A. Dehbi, A CFD model for particle dispersion in turbulent boundary layer flows, *Nucl. Eng. Des.* 238 (2008) 707–715.
- [35] H.H. Jin, J.R. Fan, M.J. Zeng, K.F. Cen, Large eddy simulation of inhaled particle deposition within the human upper respiratory tract, *J. Aerosol Sci.* 38 (2007) 257–268.
- [36] H.H. Jin, C. He, L. Lu, J.R. Fan, Numerical investigation of the wall effect on airborne particle dispersion in a test chamber, *Aerosol Air Qual. Res.* 13 (2013) 786–794.
- [37] S.V. Partankar, *Numerical Heat Transfer and Fluid Flow*, Hemisphere, Washington, DC, 1980.
- [38] N.B. Wood, A simple method for the calculation of turbulent deposition to smooth and rough surfaces, *J. Aerosol Sci.* 12 (1981) 275–290.
- [39] S.K. Friedlander, H.F. Johnstone, Deposition of suspended particles from turbulent gas streams, *Ind. Eng. Chem.* 49 (1957) 1151–1156.
- [40] A.K. Postma, L.C. Schwendiman, *Studies in Micrometrics: I. Particle Deposition in Conduits as a Source of Error in Aerosol Sampling*, Report HW-65308, Hanford Laboratory, Richland, Washington, 1960.
- [41] Z.F. Tian, K. Inthavong, J.Y. Tu, G.H. Yeoh, Numerical investigation into the effects of wall roughness on a gas-particle flow in a 90° bend, *Int. J. Heat Mass Transfer* 51 (5–6) (2008) 1238–1250.
- [42] K. Sun, L. Lu, H. Jiang, A computational investigation of particle distribution and deposition in a 90° bend incorporating a particle-wall model, *Build. Environ.* 46 (6) (2011) 1251–1262.
- [43] H. Jiang, L. Lu, K. Sun, Experimental study and numerical investigation of particle penetration and deposition in 90 degrees bent ventilation ducts, *Build. Environ.* 46 (2011) 2195–2202.